Progress In Electromagnetics Research B, Vol. 29, 1–22, 2011

SYMMETRICAL PYRAMIDAL HORN ANTENNAS BASED ON EBG STRUCTURES

I. Khromova, I. Ederra, and R. Gonzalo

Antenna Group
Public University of Navarra, Pamplona, Navarra E31006, Spain

B. P. de Hon

Department of Electrical Engineering
Eindhoven University of Technology
5600 MB Eindhoven, The Netherlands

Abstract—This paper presents a novel pyramidal (EH) horn antenna based on Electromagnetic Band Gap structures (EBGs). The reported pyramidal woodpile-based horn antenna possesses a symmetrical radiation pattern and a wide operating frequency range. Such antennas can substitute metallic horns in certain circumstances, which is especially valuable for millimetre and THz devices. The principle of creating EH-horn antennas in the woodpile structure is explained in detail. In particular, this paper presents the design of a symmetrical woodpile EH-horn antenna operating at frequencies around 110 GHz. The reported antenna exhibits a wide operating bandwidth (more than 10%), while possessing high directivity and radiation efficiency equal to 16.35 dBi and −0.55 dB (88%) respectively.

1. INTRODUCTION

In recent years, a great part of scientific and engineering research has been aimed at designing and fabricating novel microwave and optical devices based on Electromagnetic Band Gap structures (EBGs) [1–6], also known as photonic crystals. These devices open a new chapter in the world of microwave and THz applied science and engineering as they offer new advantages, such as avoiding metals or allowing for integrated devices. The great effort in creating new concepts of use and

Received 4 February 2011, Accepted 7 March 2011, Scheduled 14 March 2011
Corresponding author: Irina Khromova (irina.khromova@unavarra.es).

precise fabrication techniques promises to result in a real breakthrough for various fields of applications [7–11].

An EBG structure is a periodic, normally dielectric structure with certain geometry and dimensions, exhibiting in its spectral behavior a so called band gap — a range of frequencies, at which electromagnetic waves are not allowed to propagate in the structure. The EBGs, known also as photonic crystals in optics, have been attracting attention since decades ago. Having found almost no application in radio-physics and having triumphed in optics, they are now penetrating into the world of microwave and THz engineering, where the EBG technology opens up the possibility of creating compact and well-matched devices.

The EBGs have already been widely exploited for antenna-related applications. They were used as substrates, superstrates and coatings for shaping and improving the radiation characteristics of antennas of different types [12–17]. In particular, their ability of confining and guiding electromagnetic energy has opened up new applications and solutions in microwave and optical devices design. These novel concepts can be realized in EBGs with cavities or defects [2–5, 18, 19], which can function as resonators, waveguides and even horn antennas. Point defects in EBGs were applied to antennas in order to achieve larger directivities and higher efficiencies [20–22]. These compact defect-based antennas however resulted to be limited in terms of their operating bandwidth.

As demonstrated in [23–28], EBG structures themselves can serve as novel type of horn antennas, when a corresponding pyramidal-shaped hollow defect is introduced in the periodic structure. This hollow defect should provide an adiabatic transition between a feeding EBG waveguide and the free space. In the above cited papers creating a gradual tapering of hollow waveguides in a woodpile structure [29, 30] was proposed. The horn is realized within one woodpile layer by bending the woodpile rods, parallel to the direction of energy propagation. In this way a radiating aperture within the containing woodpile slab can be created.

Among the main interesting and promising propertied of EBG horn antennas there are the large operating bandwidth (equal to the bandwidths of the feeding EBG waveguides in two-dimensional (2D) systems [23] and comparable to the ones in three-dimensional (3D) cases); high directivity levels controlled by the horn antenna flare angles; low losses at high frequencies due to the absence of metals (provided the EBG structure is fabricated with sufficient precision); and scalability of the antenna designs, which allows one to use the same concepts for very different frequency ranges.

Despite offering a wide spectrum of applications the EBG horn

antennas in their present form (implemented by introducing a layer of bend dielectric rods in the embedding woodpile structure) still have several fundamental drawbacks.

Until now only sectoral H-horn antennas based on 3D EBG structures have been designed. In the proposed configurations the electric field is parallel to the woodpile stacking direction. Thus the E-plane dimensions of such horn antennas are determined by the thickness of the woodpile bars, since these horns are created within a single woodpile layer. Such a narrow and pre-determined aperture leads to a broad beam in the E-plane, which besides is non-symmetrical due to the absence of mirror symmetry in the stacking direction of the woodpile structure. However, the linear array proposed in [27] and the evanescently fed array proposed in [28] can improve the E-plane radiation pattern of the system.

Reducing the E-plane beamwidth would require creating a pyramidal horn antenna. The difficulty of creating a pyramidal horn based on a defect-containing woodpile structure lies in the complexity of the embedding medium itself. Looking at the woodpile structure, one can easily notice that simply bending the rods in both E- and H-plane cannot provide us with a proper pyramidal horn defect.

Even an H-horn realized as a defect in several adjacent woodpile layers cannot be designed in a straightforward way as it will be demonstrated below. Yet such an antenna would be a solution when using EBG waveguides, implemented as hollow defects in several adjacent layers of the woodpile structure. For instance, a three-layer woodpile waveguide [10], which can be well-matched to standard metallic input/output waveguides, would be coupled to a three-layer woodpile horn antenna in a more natural way than to a single-layer woodpile horn antenna.

This paper presents a solution to the above stated problem related to the absence of symmetry in the EBG horn antennas, and also proposes an approach, allowing one to create a pyramidal EBG horn antenna. Firstly, the main difference between a metallic horn antenna and an EBG horn antenna is given. It is explained why a simple and straightforward introduction of a horn-shaped defect cannot create an EBG horn antenna. Ways of realizing symmetrical horns and horns with apertures in both E- and H-planes within woodpile slabs are presented. Finally, the effect of the tolerances in the performance of such antennas is also studied.

For all the configurations of the EBG horn antennas presented in this paper the following woodpile structure parameters were chosen: period $a = 1\,\text{mm}$, woodpile rods width $d_1 = 0.3\,\text{mm}$ and height $d_2 = 0.33\,\text{mm}$. The structure is made of silicon with dielectric

permittivity 11.9. This woodpile exhibits a band gap at around 95–125 GHz. However, all the proposed structures are scalable and the same principles and ideas can be applied to antennas operating at different frequency ranges.

2. PROPERTIES OF EBG HORN ANTENNAS

In order to understand the behavior of the EBG horn antennas, it is necessary to understand, first of all, that the field structure inside an EBG horn antenna, EBG waveguide or EBG cavity, is by no means analogous to the one inside metallic horns, waveguides or resonators. However, there is an evident resemblance between those two, and this fact allows the above mentioned devices to function in a similar way. Adiabatic widening of a metallic waveguide results in creating at each point along the direction of energy propagation a local effective waveguide, which supports a fundamental mode at a frequency lower than the frequency of the fundamental mode of the initial feeding waveguide. At the same time, if the widening is gradual enough, it is possible to propagate the initial fundamental mode along the horn adapting its shape to something resembling a plane wave.

In the woodpile case when a multiple-layer antenna is looked for, bending the rods in just one layer is not enough. As has been already mentioned, a horn antenna can be created in the woodpile by simply cutting out a defect in several adjacent layers of a woodpile structure, as shown in Figure 1. However, this defect does not provide a proper

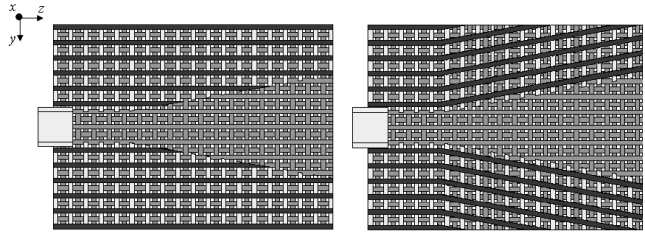

Figure 1. An H-plane cross-section view of (a) an EBG H-horn antenna realized by directly cutting out a pyramidal-shaped defect from three adjacent layers of the woodpile structure, (b) the same EBG H-horn antenna, where the middle layer of the structure was substituted by a layer of bent rods. The flare angle in both antennas is $\alpha_H = 10°$. The antennas are fed by a three-layer EBG waveguide (non-symmetrical version of the one reported in [10]), which is coupled to an input standard metallic waveguide.

functioning of the system as a horn antenna. In other words, it does not create an adiabatic transition between an EBG waveguide and the free-space due to the periodicity of the embedding structure.

In order to explain this behavior, the antenna configuration presented in Figure 1(b) will be used. It combines the bended bars in the layer where the bars are parallel to the waveguide axis, described in the literature [23–28], where well-functioning EBG horn antennas were reported, with cut bars in the top and bottom layers. However, since the EBG waveguide is periodical, the straightforward analogy of adiabatic transition in metallic horns is not applicable in this case. Even flaring it out gradually will result in an abrupt appearance of wider effective EBG waveguides (in the cross-sections of the horn antenna), which support higher-order modes.

Figure 2 demonstrates how the modal structure of the effective EBG waveguides, corresponding to certain cross-sections of a horn antenna shown in Figure 1(b), transforms while the distance from the antenna throat is increased, i.e., with the effective EBG waveguide core becoming larger. These modes were calculated at a fixed propagation constant, which was arbitrary set as $\beta = \frac{2}{3}\frac{\pi}{\lambda}$, where λ is the free space wavelength. The modes were calculated using the eigenmode solver implemented in the Ansoft HFSS software.

It can be noticed from Figure 2 that there is a general tendency, consisting in the increase of the frequencies of all the modes with the EBG waveguide core increase. This effect is similar to the one

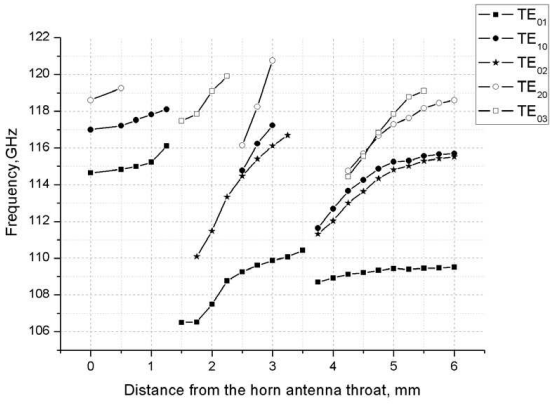

Figure 2. Modal frequencies vs. distance from the antenna throat at an arbitrary chosen propagation constant ($\beta = \frac{2}{3}\frac{\pi}{\lambda}$, where λ is the free space wavelength). Calculated for the EBG horn antenna shown in Figure 1(b).

reported in [18] and happens due to simultaneous lowering of the effective dielectric permittivity of the region occupied by the mode (in the transverse cross-section of the EBG waveguide).

At the same time, the frequencies of all the modes drop sharply at certain distances. For instance, the frequency of the TE_{01} mode drops from 116.11 GHz to 106.51 GHz at a distance of 1.5 mm from the antenna throat. This happens due to an abrupt switch between an EBG waveguide with a core occupying a lower number of EBG unit cells to an EBG waveguide with a core occupying a higher number of EBG unit cells. In this case due to larger geometrical sizes of the modes, the frequencies drop. At these distances the fundamental mode of the considered feeding EBG waveguide excites higher-order modes in the wider effective EBG waveguides, whenever the existence of these modes is permitted within the band gap, see Figure 3. As for the fact that in [23–28] the EBG horn antenna realized as a layer of bent woodpile rods functions well, one has to keep in mind that those are basically one-dimensional systems, where of course a gradual tapering is rather easy to achieve.

On the other hand, EBG waveguides are very different from metallic ones. The modes guided in EBG waveguides are not bound to the physical core boundary, as the field does not have to become zero as it does at the metallic walls. The shape of the fundamental mode of a three-layer EBG waveguide (a non-symmetrical analogy of the one reported in [10]) is however very similar to that of a metallic waveguide.

Figure 4 presents the profiles of the modes whose dispersion

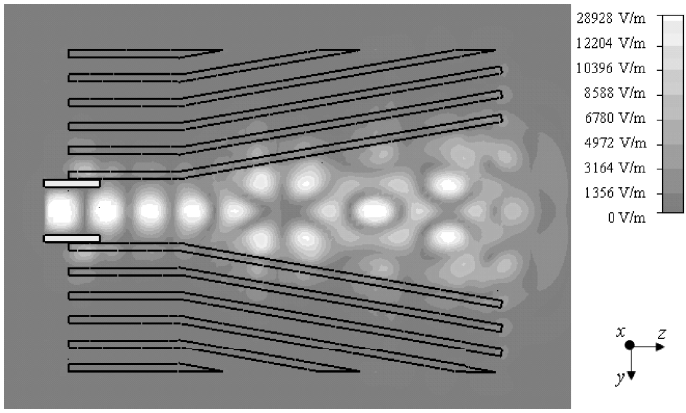

Figure 3. Typical field pattern in the H-plane cross-section of the antenna shown in Figure 1(b).

characteristics are shown in Figure 2. It can be noticed that the structures of the fields do not exactly correspond to those of the metallic waveguide modes. Still one can figure out the order of the mode by noting the number of zeros in each direction. The modes are not strictly TE modes, however due to certain resemblance they are referred to as TE_{mn} modes for convenience.

While exciting the antenna with the TE_{01} mode of the EBG waveguide, one can observe the higher order modes appear within the horn (see Figure 3). Actually, the points, where these modes are excited, become the main reflecting points for the horn.

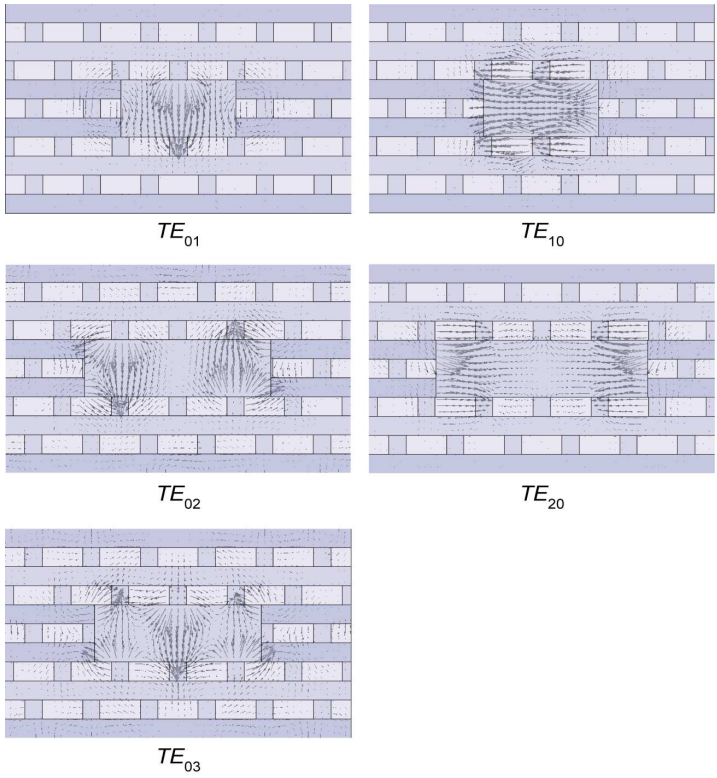

Figure 4. Electric field distribution of the modes of the effective three-layer woodpile waveguide, corresponding to certain cross-sections of the woodpile horn antenna shown in Figure 1(b). The cross-sections (and the effective EBG waveguide profiles correspondingly) are chosen arbitrarily.

3. NEW CONCEPT OF WOODPILE-BASED HORN ANTENNAS

In this paper, a solution for the problem described in the previous section is proposed. The main concept of providing an adiabatic transition between a waveguide and the free-space lies in creating real "EBG-walls" analogous to metallic walls in conventional horn antennas. It can be done by turning the whole EBG structure at an angle equal to horn antenna flare angle (Figure 5). Doing so, one shifts all the nodes of the EBG lattice and avoids creating larger EBG waveguides along the direction of wave propagation. Instead an "EBG wall" appears around the horn antenna, where the reflection happens due to the band gap effect and at each position along the horn the wave faces the same boundary conditions. In such a system the field behaves in principle in the same way as it does within a metallic horn antenna.

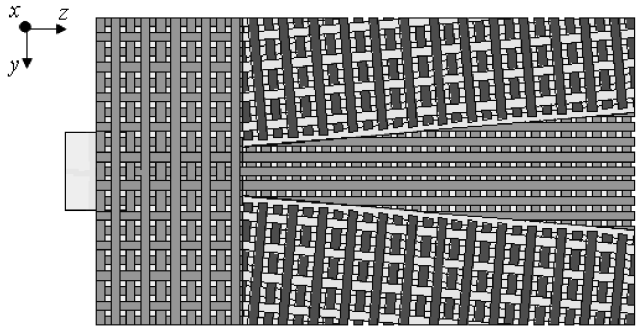

Figure 5. A woodpile-based H-horn antenna realized by turning the EBG "walls" at the antenna flare angle (10°).

Figure 6 shows how the modal frequencies of the effective EBG waveguide (corresponding to certain cross-sections of the horn antenna shown in Figure 5) change with the increase of the distance from the antenna throat. As those in Figure 2, the modes in Figure 6 were calculated at a fixed propagation constant $\beta = \frac{2}{3}\frac{\pi}{\lambda}$, where λ is the free space wavelength.

Unlike the previous case the frequencies of the modes in Figure 6 decrease with the increase of the effective EBG waveguide size. At the same time there are no sudden drops in the modal frequencies and thus, once excited, a mode inside this EBG horn antenna is not likely to break up into higher-order modes. The single-layer EBG antenna with bent rods [26–28] realizes the same principle within one woodpile layer.

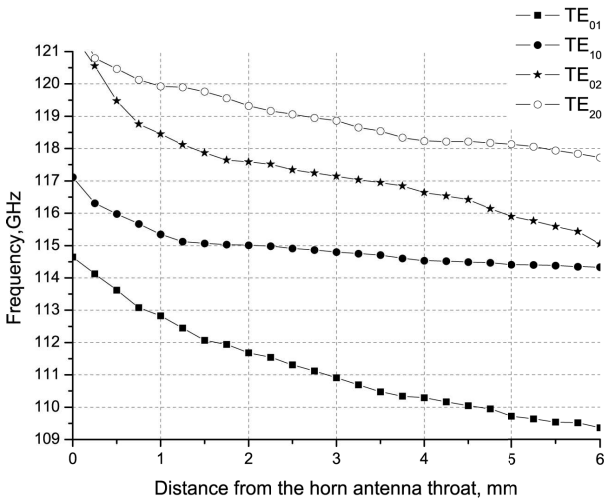

Figure 6. Modal frequencies vs. distance from the antenna throat at an arbitrary chosen propagation constant $\beta = \frac{2}{3}\frac{\pi}{\lambda}$, where λ is the free space wavelength. Calculated for the EBG horn antenna shown in Figure 5.

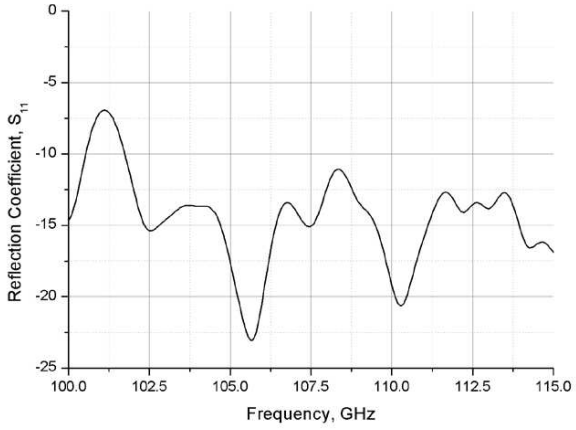

Figure 7. Input reflection coefficient of the three-layer woodpile H-horn antenna. Flare angle $\alpha_E = 10°$.

Analogous to the resonators, where the EBG walls are pushed apart [18], the above mentioned fact allows the structure to avoid the generation of higher-modes. The reflection coefficient and the

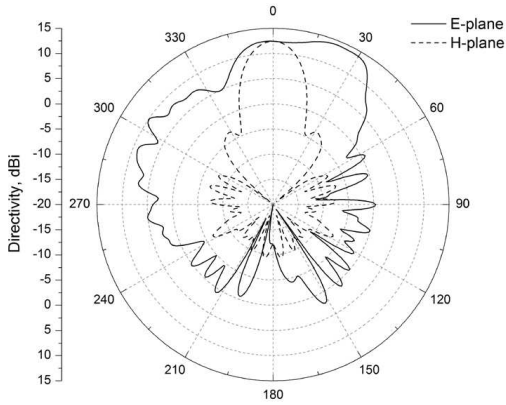

Figure 8. Radiation pattern of the three-layer woodpile H-horn antenna at 110 GHz.

typical antenna radiation pattern, for a 10° flare angle are presented in Figure 7 and Figure 8. These results were obtained when the waveguide was fed by a standard metallic WR8 waveguide. In this work, the EBG horn antennas were simulated using the FDTD method (provided by CST Microwave Studio).

It can be noticed that as expected from [26–28] the radiation pattern is not symmetrical in the E-plane due to lack of symmetry of the woodpile in the stacking direction, as aforementioned. However, a mirror-symmetry in the woodpile stacking direction can be introduced in order to achieve symmetrical radiation pattern. For instance, this would allow one to use a symmetrical three-layer EBG waveguide [10] as a feed.

4. WOODPILE-BASED SYMMETRICAL PYRAMIDAL HORN ANTENNA

The proposed method of bending the whole EBG structure for creating a proper adiabatic transition for horn antennas can be applied to a woodpile-based pyramidal horn antenna design. In order to realize a pyramidal horn based on a defect-containing woodpile, the idea is to create EBG walls in both vertical and horizontal directions by means of turning the EBG structure in both E- and H-plane (Figure 9).

The proposed configuration functions as a pyramidal horn antenna and can be used as an analogy of a classical metallic horn when needed (for instance, at high frequencies or in integrated EBG-based systems). A parametrical analysis has been carried out in order to determine the

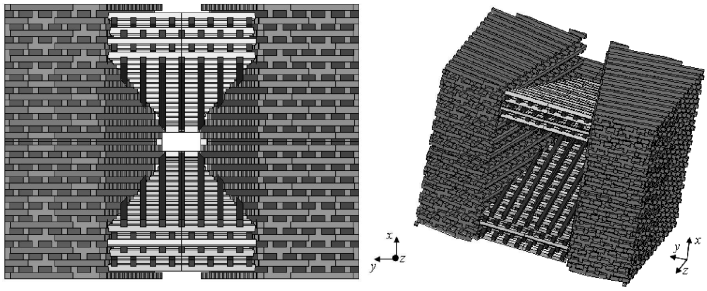

(a) (b)

Figure 9. Woodpile based symmetrical EH-horn antenna ((a) front view, (b) 3D view). The flare angles in the E- and H-planes were both set as $\alpha_E = \alpha_H = 12.5°$.

Table 1. Operating bandwidth (in %) of the symmetrical pyramidal EBG horn antenna at different flare angles in E- and H-planes.

α_H/α_E,°	5	7.5	10	12.5	15
5	4.86	4.01	6.09	9.34	7.38
7.5	7.41	9.25	8.86	10.24	6.74
10	6.64	10.51	9.57	10.59	7.59
12.5	7.78	10.56	10.46	10.75	8.17
15	8.60	7.46	8.20	9.38	10.06

impact of the flare angle on the antenna performance. Tables 1–3 illustrate the results of this analysis.

Table 1 presents the estimated operating bandwidth of the symmetrical pyramidal woodpile-based horn antenna for different E- and H-plane flare angles. The broadest bandwidth is achieved at $\alpha_E = \alpha_H = 12.5°$. The operating frequency band was determined as a frequency range, where the reflection coefficient of the antenna stays below -10 dB and where the peak directivity of the antenna does not drop away for more than -3 dBi from its maximum value. When increasing the flare angles, at a certain point the performance of the antenna becomes worse. The best way to explain this fact is to imagine that at this point the transition between the EBG waveguide and the free space becomes too abrupt and, thus, at certain frequencies, the level of reflection increases narrowing the operating bandwidth of the antenna. At the same time when a smooth waveguide-to-free-space transition becomes abrupt, the field pattern may change (instead of repeating the fundamental mode pattern it tends to break up into

Table 2. Peak directivity (dBi) of the symmetrical pyramidal EBG horn antenna at different flare angles in E- and H-planes.

α_H/α_E,°	5	7.5	10	12.5	15
5	11.84	12.51	13.56	14.13	14.70
7.5	12.77	14.21	15.23	15.82	16.82
10	15.09	15.45	16.31	17.13	17.75
12.5	13.39	15.46	16.17	16.35	17.39
15	12.51	14.98	16.62	16.97	16.79

Table 3. Difference between beamwidths (in °) in E- and H-planes of the symmetrical pyramidal EBG horn antenna at different flare angles in E- and H-planes at frequencies corresponding to peak directivity level.

α_H/α_E,°	5	7.5	10	12.5	15
5	5	27.4	11.3	38.7	7.6
7.5	30.7	15.11	8.2	1.5	8.5
10	27	7.9	9.4	0.9	2.2
12.5	35.8	8.6	8.8	2	4
15	28.2	11.1	8.5	4.7	1.6

higher order modes), which can lead to lower directivity levels and splitting of the main lobe into two or more lobes.

Studying the peak directivity of the antenna presented in Table 2 and the difference between E- and H-plane beamwidths together with the results presented in Table 1 permits one to conclude that the performance of the antennas with $\alpha_E = \alpha_H = 12.5°$ and $\alpha_E = \alpha_H = 15°$ are comparable in terms of the parameters concerned. Moreover, according to Table 3 the antenna appears to be slightly more directive when $\alpha_E = \alpha_H = 15°$(22.1° in the E-plane and 23.7° in the H-plane) than when the flare angles are $\alpha_E = \alpha_H = 12.5°$(23° in E-plane and 25° in the H-plane). However, in terms of the radiation pattern and the level of side lobes the latter can still be given preference. Figure 10 compares the level of the side lobes throughout the operating bandwidths of the two antennas, and it can be noticed that in the frequency range around 107–110 GHz in the H-plane it stays around −3 dBi lower for the antenna with $\alpha_E = \alpha_H = 12.5°$ when compared to that of the wider flare angle antenna configuration.

The E- and H-plane flare angles of the antenna shown in Figure 9

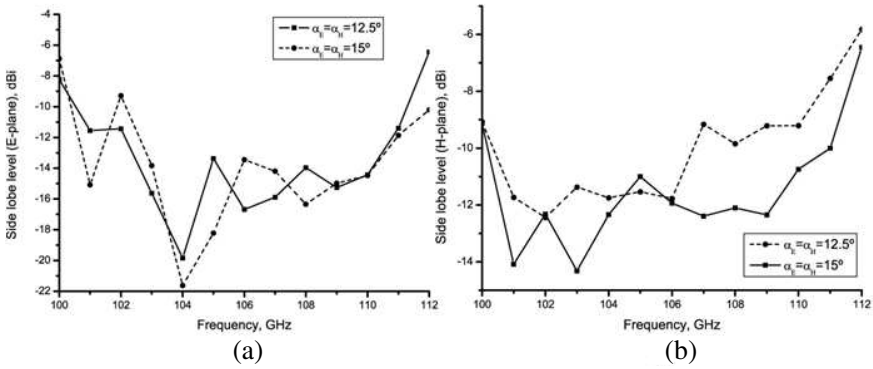

Figure 10. Side lobes level for (a) E- and (b) H-plane within the operating frequency band of the symmetrical pyramidal EBG horn antenna.

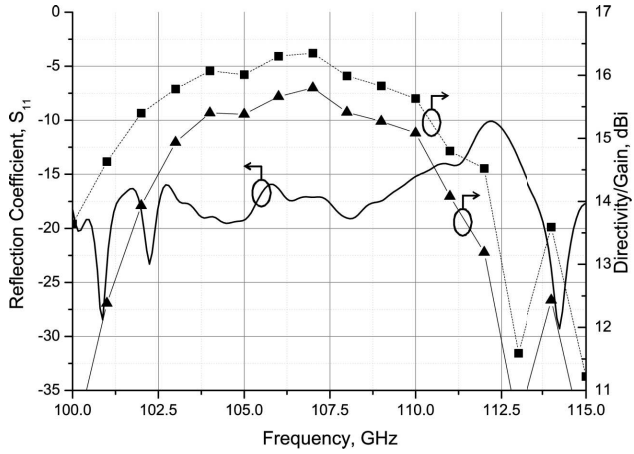

Figure 11. Input reflection coefficient (black solid curve), peak directivity value (dashed curve with black squares) and peak gain (solid curve with black triangles) of the symmetrical woodpile EH-horn antenna.

were both set as $\alpha_E = \alpha_H = 12.5°$, as, according to parametrical analysis, this appears to be the optimal angle providing better reflection spectrum, relatively equal width of the beams in both E- and H-planes and lower side lobes. The performance of the antenna in terms of input reflection coefficient, peak directivity and gain is shown in Figure 11. The operating bandwidth of the present EBG

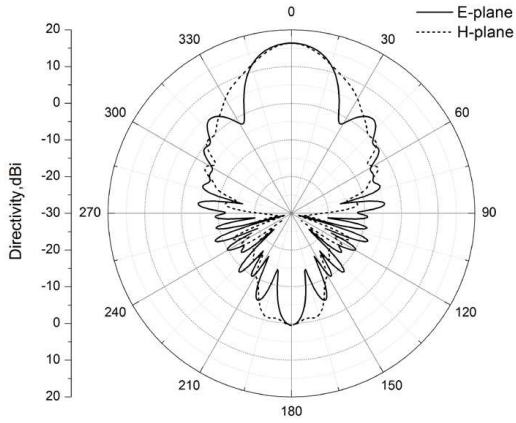

Figure 12. Radiation pattern of the symmetrical woodpile EH-horn antenna at 107 GHz.

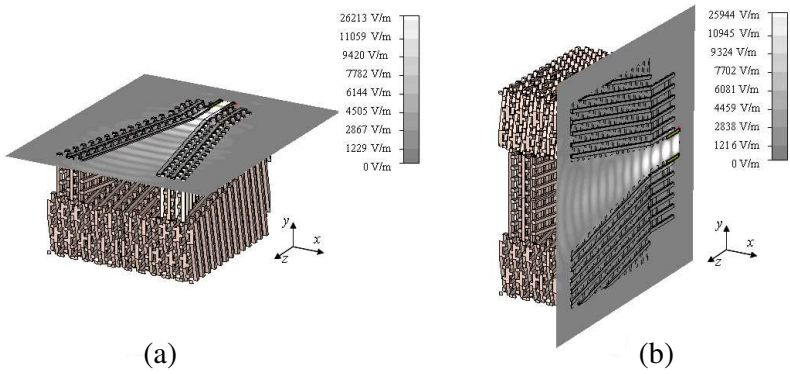

Figure 13. (a) and (b) Absolute value of electric field in E- and H-plane cross-sections respectively at $f = 107$ GHz.

horn antenna is estimated as 10.75%: in the region from 100.4 GHz to 111.8 GHz.

Figure 12 presents the radiation pattern of the proposed EBG horn antenna configuration. It can be noticed that the pattern is symmetrical in both E- and H-planes, this property could not be achieved in the previously reported configurations of the woodpile-based horn antennas.

The field distribution at 107 GHz is shown in Figure 13. It can be seen that its behavior resembles the behavior of the electric field in a metallic horn antenna, which means an adiabatic transition between

the feeding waveguide mode and the free space is achieved in the proposed EBG EH-horn antenna.

Thus, a new concept of designing woodpile-based antennas allowing one to realize pyramidal horns is presented. Turning the EBG slabs surrounding the actual core of the horn provides a gradual tapering, which means a smooth transition between the EBG feeding waveguide and the free space. The proposed pyramidal horn antenna based on a woodpile structure demonstrates good performance and competitive parameters.

The proposed pyramidal EBG horn antennas can be used for designing integrated devices based on EBG technology. They can be easily matched to other EBG-based components, such as waveguides, filters, power-splitters, etc., implemented within the same slab of the embedding periodic structure.

5. SENSITIVITY ANALYSIS

Since the performance of the EBG-based devices tends to strongly depend on the geometry of the structure, a sensitivity analysis of the proposed EBG horn antenna performance with respect to its main geometrical parameters was performed. In particular, the impact of antenna starting point with respect to the EBG waveguide and the antenna flare angle was evaluated.

Due to periodicity of the embedding medium placing the antenna throat in the optimal position with respect to the EBG waveguide is important. This optimal position should be calculated by means of a parametrical analysis for each antenna in particular. At the same time it is important to see how small errors in antenna positioning affect the performance of the system. Figure 14 presents the input reflection coefficient of the antennas, where the position of the horn throat is shifted by Δl with respect to the optimal position. Within the operating frequency band (100.4 GHz–111.8 GHz) the calculated mean, maximum and minimum error in the reflection coefficient (dimensionless) in the previous cases are given in Table 4. The reflection coefficient is slightly affected by this shift and even for a 10% error the maximum change is relatively small. Table 4 also shows the change in the peak directivity value occurring when the antenna throat is shifted from its optimal position ($\Delta\mathrm{Dir}_{\max} = \mathrm{Dir}_{\max}^{\Delta l} - \mathrm{Dir}_{\max}^{opt}$, where $\mathrm{Dir}_{\max}^{\Delta l}$ is the peak directivity of the antenna with a displaced throat and $\mathrm{Dir}_{\max}^{opt} = 16.35\,\mathrm{dBi}$ is the peak directivity of the antenna with the correct position of the throat).

Another important geometrical parameter of the horn antenna is the flare angle. In case of the pyramidal horn there are two

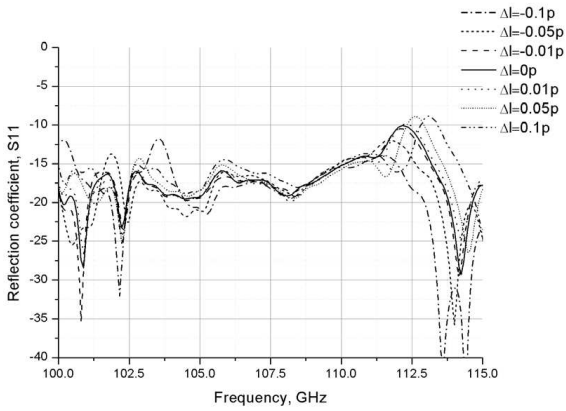

Figure 14. Input reflection coefficient of the symmetrical woodpile EH-horn antenna at different antenna throat positions Δl is the antenna throat position shift with respect to the initial one in terms of the woodpile period p.

Table 4. The mean, maximum and minimum values of the error in the reflection coefficient (ΔS_{11}^{mean}, $\Delta S_{11}^{\max}$, $\Delta S_{11}^{\min}$) and the error in the peak directivity $\Delta\mathrm{Dir}_{\max}$ dB of the pyramidal EBG horn antenna at different antenna throat positions.

Δl,%	ΔS_{11}^{mean}	$\Delta S_{11}^{\max}$	$\Delta S_{11}^{\min}$	$\Delta\mathrm{Dir}_{\max}$,dB
-10	0.00799	0.05114	$9.29 \cdot 10^{-5}$	0.2
-5	0.00447	0.02381	$1.29 \cdot 10^{-4}$	0.12
-1	0.0014	0.00554	$1.95 \cdot 10^{-5}$	0.05
1	0.00155	0.00841	$1.03 \cdot 10^{-6}$	-0.05
5	0.00548	0.04808	$1.39 \cdot 10^{-5}$	-0.012
10	0.00688	0.05325	$2.4 \cdot 10^{-5}$	-0.19

angles, one corresponding to the flaring in the E-plane (α_E) and one corresponding to the flaring in the H-plane (α_H). Figure 15 and Figure 16 demonstrate how the input reflection coefficient depends on the error in the flare angles of the antenna ($\Delta\alpha_E$ and $\Delta\alpha_H$ correspondingly).

The calculated mean, maximum and minimum error in the reflection coefficient (dimensionless) within the operating frequency band for $\pm 1^\circ$ and $\pm 0.5^\circ$ change in the E-plane flare angle are given in Table 5. It also presents the changes in peak directivity values at different E-plane flare angles ($\Delta\mathrm{Dir}_{\max} = \mathrm{Dir}_{\max}^{\Delta\alpha_E} - \mathrm{Dir}_{\max}^{opt}$, where

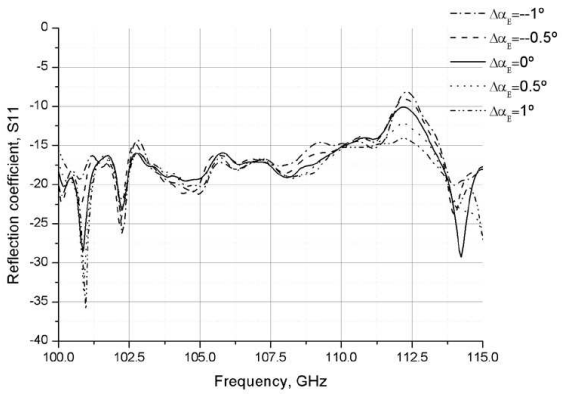

Figure 15. Sensitivity of the input reflection coefficient of the symmetrical woodpile EH-horn antenna towards the change in the E-plane flare angle ($\Delta\alpha_E$) with respect to the initial one (12.5°).

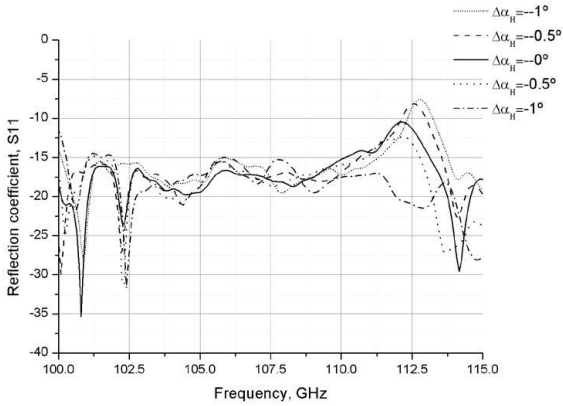

Figure 16. Sensitivity of the input reflection coefficient of the symmetrical woodpile EH-horn antenna towards the change in the H-plane flare angle ($\Delta\alpha_H$) with respect to the initial one (12.5°).

$\mathrm{Dir}_{\max}^{\Delta\alpha_E}$ is the peak directivity of the antenna with an error in the E-plane flare angle and $\mathrm{Dir}_{\max}^{opt} = 16.35\,\mathrm{dBi}$ is the peak directivity of the antenna with the correct E-plane flare angle).

The calculated mean, maximum and minimum error in the reflection coefficient (dimensionless) within the operating frequency band for ±1° and ±0.5° change in the H-plane flare angle are given in Table 6. As in the previous case variations of 1° do not significantly

Table 5. The mean, maximum and minimum values of the error in the reflection coefficient (ΔS_{11}^{mean}, $\Delta S_{11}^{\max}$, $\Delta_{11}^{\min}$) and the error in the peak directivity $\Delta\mathrm{Dir}_{\max}$,dB of the pyramidal EBG horn antenna at different antenna E-plane flare angles.

$\Delta\alpha_E$,°	$\Delta\mathrm{S}_{11}^{mean}$	$\Delta S_{11}^{\max}$	$\Delta S_{11}^{\min}$	$\Delta\mathrm{Dir}_{\max}$,dB
-1	0.00141	0.01512	$1.24 \cdot 10^{-3}$	-0.21
-0.5	0.00272	0.00892	$1.15 \cdot 10^{-4}$	-0.1
0.5	0.00195	0.02933	$9.82 \cdot 10^{-7}$	0.33
1	0.00345	0.04401	$1.71 \cdot 10^{-5}$	0.43

Table 6. The mean, maximum and minimum values of the error in the reflection coefficient (ΔS_{11}^{mean}, $\Delta S_{11}^{\max}$, $\Delta S_{11}^{\min}$) and the error in the peak directivity $\Delta\mathrm{Dir}_{\max}$,dB of the pyramidal EBG horn antenna at different antenna H-plane flare angles.

$\Delta\alpha_H$,°	$\Delta\mathrm{S}_{11}^{mean}$	$\Delta S_{11}^{\max}$	$\Delta S_{11}^{\min}$	$\Delta\mathrm{Dir}_{\max}$,dB
-1	0.00552	0.03002	$2.46 \cdot 10^{-5}$	-0.26
-0.5	0.005	0.01866	$1.47 \cdot 10^{-4}$	0.01
0.5	0.00452	0.02469	$6.08 \cdot 10^{-5}$	0.04
1	0.01023	0.06745	$1.14 \cdot 10^{-4}$	0.25

affect the performance of the antenna. It also presents the changes in peak directivity values at different H-plane flare angles $\Delta\mathrm{Dir}_{\max} = \mathrm{Dir}_{\max}^{\Delta\alpha_H} - \mathrm{Dir}_{\max}^{opt}$, where $\mathrm{Dir}_{\max}^{\Delta\alpha_H}$ is the peak directivity of the antenna with an error in the H-plane flare angle and $\mathrm{Dir}_{\max}^{opt} = 16.35\,\mathrm{dBi}$ is the peak directivity of the antenna with the correct H-plane flare angle.

The major deviations of the reflection coefficient value concentrate predominantly at the edges of the operating frequency band of the EBG EH-horn antenna as it can be seen on Figure 14, Figure 15 and Figure 16. Taking this fact into account, one can say that in terms of input reflection the proposed EBG horn appeared to be robust towards significant errors in horn defect positioning with respect to the feeding EBG waveguide and towards the changes in the flare angle.

The variations of the directivity with the indicated changes in flare angles and antenna throat position are of order of tenths of dB. This allows one to conclude that in terms of directivity the pyramidal EBG horn antenna is also rather robust towards errors in structure geometry.

6. CONCLUSION

In this paper, a novel pyramidal EBG horn antenna design and concept was presented. Previously reported woodpile based horn antennas were restricted to be sectoral since the embedding medium did not allow to create apertures in both E- and H-planes by bending the woodpile bars. Moreover, the woodpile based horn antennas used to have a non-symmetrical radiation pattern due to the absence of mirror symmetry in the stacking direction of the embedding periodic structure. The concept presented in this paper lies in combining EBG slabs turned at different angles in order to form a horn antenna. This approach allows one to create apertures in both E- and H-planes and also to introduce symmetries which the embedding woodpile medium does not possess. Thus, a pyramidal woodpile-based horn antenna with a symmetrical radiation pattern can be designed.

We have shown that in order to provide an adiabatic transition between an EBG waveguide and the free-space, one has to turn the whole EBG structure at an angle equal to horn antenna flare angle and to create a slow and gradual aperture. Otherwise, if the lattice nodes are not displaced along the way from the antenna throat to the antenna aperture, the abrupt changes in the horn cross-sections make the initial electromagnetic mode break up into higher-order modes.

An F band silicon woodpile-based pyramidal horn antenna was designed following this idea. The presented antenna operates within 100.4 GHz–111.8 GHz according to the numerical simulation results and thus exhibits a 10.2% bandwidth. Its competitive parameters demonstrate also that such EBG-based components can be considered when designing integrate EBG-based devices and can serve as alternatives of metallic horns in certain situations. The presented antenna thanks to certain degree of scalability of the overall system can be re-designed for different ranges of frequencies provided a proper material and dimensions are used for the embedding woodpile structure design.

ACKNOWLEDGMENT

Supported by the Spanish Ministry of Science and Innovation Project Nos. TEC2009-11995 and CSD2008-00066.

REFERENCES

1. Yablonovitch, E., "Inhibited spontaneous emission in solid-state physics and electronics," *Phys. Rev. Lett.*, Vol. 58, 2059–2062,

1987.

2. John, S., "Strong localization of photons in certain disordered dielectric superlattices," *Phys. Rev. Lett.*, Vol. 58, 2486, 1987.
3. Meade, R. D., K. D. Brommer, A. M. Rappe, and J. D. Joannopoulos, "Photonic bound states in periodic dielectric materials," *Phys. Rev. B*, Vol. 44, No. 24, 13772–13774, 1991.
4. Joannopoulos, J. D., R. D. Meade, and J. N. Winn, *Photonic Crystals*, Princeton University Press, 1995.
5. Joannopoulos, J. D., P. R. Villeneuve, and S. Fan, "Photonic crystals: Putting a new twist on light," *Nature*, Vol. 386, 143, 1997.
6. Ho, K. M., C. T. Chan, and C. M. Soukoulis, "Existence of a photonic gap in periodic dielectric structures," *Phys. Rev. Lett.*, Vol. 65, 3152, 1990.
7. Ederra, I., R. Gonzalo, C. Mann, and P. de Maagt, "(Sub)mmwave components and subsystems based on PBG technology," *Proc. IEEE AP-S Int. Symp. Dig.*, 1087–1090, 2003.
8. Ederra, I., et al., "EBG millimetre-wave components design," *Proc. 3rd ESA Workshop on Millimetre Wave Technology and Applications*, 129–134, Espoo, Finland, May 21–23, 2003.
9. Ederra, I., et al., "Measurements of sub-mm and mm-wave components and subsystems based on EBG technology," *Proc. 3rd ESA Workshop on Millimetre Wave Technology and Applications*, 459–464, Espoo, Finland, May 21–23, 2003.
10. Ederra, I., I. Khromova, R. Gonzalo, N. Delhote, D. Baillargeat, A. Murk, B. E. J. Alderman, and P. de Maagt, "Electromagnetic band gap waveguide for the millimeter range," *IEEE Trans. on Microwave Theory and Techniques,* Vol. 58, No. 7, 1734–1741, 2010.
11. De Maagt, P., R. Gonzalo, Y. C. Vardaxoglou, and J. M. Baracco, "Electromagnetic bandgap antennas and components for microwave and (sub)millimeter wave applications," *IEEE Trans. Antennas Propag.*, Vol. 51, No. 10, 2667–2677, 2003.
12. Brown, E. R., C. D. Parker, and E. Yablonovitch, "Radiation properties of a planar antenna on a photonic-crystal substrate," *J. Opt. Soc. Am. B*, Vol. 10, No. 2, 404–407, 1993.
13. Gonzalo, R., I. Ederra, C. M. Mann, and P. de Maagt, "Radiation properties of terahertz dipole antenna mounted on photonic crystal," *Electronics Letters*, Vol. 37, No. 10, 613–614, May 2001.
14. Ederra, I., R. Gonzalo, B. E. J. Alderman, P. G. Huggard, B. P. de Hon, M. C. van Beurden, A. Murk, L. Marchand, and

P. Maagt, "Electromagnetic band gap based planar imaging array for 500 GHz," *IEEE Trans. on Microwave Theory and Techniques*, Vol. 56, No. 11, 2556–2565, Nov. 2008.

15. Kesler, M. P., J. O. Maloney, and B. L. Shirley, "Antenna design with the use of photonic band-gap materials as all-dielectric planar reflectors," *Microwave and Opt. Technology Lett.*, Vol. 11, No. 4, 169–174, 1996.
16. Smith, G. S., M. P. Kesler, and J. G. Maloney, "Dipole antennas used with all-dielectric, woodpile photonic-bandgap reflectors: Gain, field patterns, and input impedance," *Microwave Opt. Technol. Lett.*, Vol. 21, No. 3, 191–196, 1999.
17. Zhao, Z., Q. Deng, H. Xu, C. Du, and X. Luo, "A sectoral horn antenna based on the electromagnetic band-gap structures," *Microwave and Opt. Technology Lett.*, Vol. 50, No. 4, 965–969, 2008.
18. Khromova, I., R. Gonzalo, I. Ederra, and P. de Maagt, "Resonance frequencies of cavities in three-dimensional electromagnetic band gap structures," *Journal of Appl. Phys.*, Vol. 106, No. 1, 014901-1–7, 2009.
19. Ozbay, E., B. Temelkuran, and M. Bayindir, "Microwave applications of photonic crystals," *Progress In Electromagnetics Research*, Vol. 41, 185–209, 2003.
20. Serier, C., C. Cheype, R. Chantalat, M. Thevenot, T. Monediere, A. Reinex, and B. Jecko, "1-D photonic bandgap resonator antenna," *Microwave Opt. Technol. Lett.*, Vol. 29, No. 5, 312–315, 2001.
21. Cheype, C., C. Serier, M. Thevenot, T. Monediere, A. Reinex, and B. Jecko, "An electromagnetic bandgap resonator antenna," *IEEE Trans. Antennas Propag.*, Vol. 50, No. 9, 1285–1290, 2002.
22. Biswas, R., E. Ozbay, B. Temelkuran, M. Bayindir, M. M. Sigalas, and K. M. Ho, "Exceptionally directional sources with photonic-bandgap crystals," *J. Opt. Soc. Am. B*, Vol. 11, 1684–189, 2001.
23. Weily, A. R., K. P. Esselle, and B. C. Sanders, "Photonic crystal horn and array antennas," *Phys. Rev. E*, Vol. 68, 016609-1–016609-6, 2003.
24. Moore, R. L., M. P. Kesler, J. G. Maloney, and B. L. Shirley, US Patent 5,689,275, 1997.
25. Weily, A. R., K. P. Esselle, B. C. Sanders, and T. S. Bird, "High-gain 1d ebg resonator antenna," *Microwave and Opt. Technology Lett.*, Vol. 47, No. 2, 107–114, 2005.
26. Weily, A. R., K. P. Esselle, and B. C. Sanders, "Layer-by-layer

photonic crystal horn antenna," *Phys. Rev. E*, Vol. 70, 037602-4, 2004.

27. Weily, A. R., K. P. Esselle, T. S. Bird, and B. C. Sanders, "Linear array of woodpile EBG sectoral horn antennas," *IEEE Trans. Antennas Propag.*, Vol. 54, No. 8, 2263–2274, 2006.
28. Khromova, I., I. Ederra, J. Teniente, R. Gonzalo, and K. Esselle, "Evanescently-fed electromagnetic band gap horn antennas and arrays," *IEEE Trans. Antennas Propag.*, 2010.
29. Ho, M., C. T. Chan, C. M. Soukoulis, R. Biswas, and M. Sigalas, "Photonic band gaps in three dimensions: New layer-by-layer periodic structures," *Solid State Commun.*, Vol. 89, No. 6, 413–416, 1994.
30. Sözüer, H. S. and J. Dowling, "Photonic band calculations for woodpile structures," *J. Mod. Opt.*, Vol. 41, No. 2, 231–239, 1994.